COGENETIC ZIRCON, MONAZITE, XENOTIME, AND FLUORAPATITE FROM APOPICRITIC PHLOGOPITE–MAGNESITE GUMBEITES AT THE BEREZOVSKY GOLD DEPOSIT, URALS, RUSSIA

Ernst M. Spiridonov
Faculty of Geology, Lomonosov Moscow State University, Moscow, Russia, ernstspiridon@gmail.com
Inna M. Kulikova
Institute of Mineralogy, Geochemistry, and Crystal Chemistry of Rare Elements, Moscow, Russia, kulikova@imgre.ru
Firat M. Nurmukhametov
Ural Geological Museum, Yekaterinburg, Russia, museum@usmga.ru
Nina V. Sidorova
Faculty of Geology, Lomonosov Moscow State University, Moscow, Russia
Natalya N. Korotaeva
Faculty of Geology, Lomonosov Moscow State University, Moscow, Russia
Yurii A. Polenov
Institute of Geology and Geophysics, Ural State Mining University, Yekaterinburg, Russia, igggl@ursmu.ru
Alevtina N. Troshkina
Berezovsky Mine, Berezovsky, Sverdlovsk region, info@ooobru.ru

Listvenite-like phlogopite-magnesite gumbeites, a new type of gumbeites at the Berezovsky gold deposit, Urals replaced deformed zinc chromite- and ilmenite-bearing variolitic picrite enriched in Ti, P, Ce, La, Nd, Y, U, Th, and Nb. This metasomatic rock is composed of Mn- and Ca-poor magnesite ($Mg_{83-91}Fe_{9-17}$), quartz, fluorphlogopite, potassium feldspar ($K_{94-97}Na_{3-6}$), albite ($Na_{98.5}Ca_1K_{0.5}$), muscovite enriched in F, rutile, chlorite ± dravite, dolomite, fluorapatite, monazite, zircon, xenotime, gersdorffite, siegenite, millerite, Co-bearing pyrite, and galena. Talc-magnesite altered rock of the outer zone contains hematite, hydroxylphlogopite, hydroxylapatite, and violarite. Clusters of fluorapatite, monazite, zircon and xenotime are intergrown with aggregates of rutile replacing deformed plates of ilmenite; the crystals of these minerals have compromise growth surface with quartz and magnesite. Dominant zones of zircon crystals contain 1.4–1.9 wt.% Hf and traces of U, Th, Y; zones enriched in U contain up to, wt.%: 3.8 U, 2.4 Hf, 1.4 Y, 0.8 Th, U/Th is 3–9. The composition of U-free and Th-poor (0.8–2.2 wt.% Th) monazite corresponds to the formula $(Ce_{0.40-0.43}La_{0.25-0.28}Nd_{0.16-0.18}Y_{0.02-0.05}Pr_{0.03}Sm_{0.02}Gd_{0.01}Eu_{0.01}Th_{0.01-0.02}Ca_{0.02})(P_{0.97-0.98}Si_{0.01-0.03})O_4$. Cores of crystals of monazite are enriched in Y; the temperature of their crystallization estimated from the Gratz-Heinrich equation (Gratz and Heinrich, 1997) is ca. 450°C, while that of rims is ca. 300°C. The composition of Th-free U-poor (0.1–0.8 wt.% U) xenotime corresponds to the formula $(Y_{0.71-0.74}Dy_{0.05-0.06}Gd_{0.04}Er_{0.03}Nd_{0.03}Yb_{0.02-0.03}Eu_{0.01}Tb_{0.01}Ho_{0.01}Lu_{0-0.01}Ca_{0-0.01})(P_{0.99-1}Si_{0.01})O_4$.
In the fluorapatite-monazite-zircon-xenotime assemblage, U is concentrated in zircon; Th is concentrated in monazite and to less extent in zircon; *LREE* and most Y are concentrated in monazite-(Ce) that is predominant over xenotime; the latter is a carrier of *HREE* and partially Y; fluorapatite is nearly *REE*- and actinide-free. Thus, the high-temperature gumbeites was found at the northern Berezovsky deposit for the first time.
12 tables, 15 figures, 58 references.
Keywords: apopicritic phlogopite-magnesite gumbeites, zircon, monazite, xenotime, apatite, tourmaline, Mg-rich muscovite, zincochromite.

Review of gumbeites formation

Gumbeites as a special type of hydrothermal metasomatites was reported for the first time by Korzhinsky (1953) at the Gumbeika scheelite deposits, South Urals, which were studied in detail by Matveev (1928). Like beresites, gumbeites is a product of CO_2 alteration. Quartz-carbonate-potassium feldspar assemblage is typical of gumbeites (Korzhinsky, 1953), whereas quartz-carbonate-muscovite assemblage is characteristic of beresites and listvenites (Karpinsky, 1887; Borodaevsky and Borodaevskaya, 1947; Sazonov, 1984; Spiridonov and Pletnev, 2002; Spiridonov, 1991). Sazonov (1984) suggested that beresites gradually changes downward to gumbeites. Grabezhev (1981) reported apogranitic gumbeites at the Berezovsky deposit for the first time. We established that at this deposit gumbeites and beresites occur at the same level without gradual transition; mineralogy and isotopic characteristics of gumbeites and associated ores differ from those of younger gold-bearing beresites; gumbeites replaced adamellite-porphyry; gumbeites is replaced by beresites and is cut by gold-bearing quartz veins (Spiridonov *et al.*, 1998_1; 2000).

Spiridonov *et al.* (1998_1) reported six varieties of the Ural gumbeites as temperature decreases: (1) biotite-calcite gumbeites accompanied

with potassium feldspar-calcite-quartz veins and bodies with molybdoscheelite, apatite, pyrite, W-rich rutile, and monazite (ca. 450–400°), (2) biotite-calcite-dolomite gumbeites accompanied with potassium feldspar-dolomite-quartz veins with Mo-rich scheelite, pyrite, apatite, W-bearing rutile (ca. 400–370°), (3) biotite-dolomite gumbeites accompanied with potassium feldspar-dolomite-quartz veins with scheelite, pyrite, molybdenite-3*R*, apatite, and chalcopyrite (ca. 370–330°), (4) dolomite gumbeites accompanied by veins with scheelite, pyrite, chalcopyrite, galena enriched in Bi, tennantite-tetrahedrite, and Bi-Pb-Cu-Ag sulfosalts (ca. 350–290°), (5) picrophengite gumbeites accompanied with veins containing pyrite, galena, sphalerite, tennantite-tetrahedrite, meneghinite, and bournonite (ca. 310–260°), and (6) ferrophengite gumbeites accompanied with adularia-calcite-quartz veins containing pyrite, galena, cleophane, tennantite-tetrahedrite, aikinite, altaite, tetradymite, hessite, native gold, andorite, and late barite, strontianite, and witherite (< 200°) (Spiridonov *et al.,* 1998$_1$). Gumbeitization is expressed as influx of CO_2, K, S, and As with SiO_2 and Na partially being removed. Phosphorous is mobile at the formation of gumbeite. It is removed and input in back zones of various alteration columns of gumbeite. The mobility of P during gumbeitization is one of the reasons to form scheelite ore because P strongly stabilizes polytungsten complexes (probable transfer species of W).

High-temperature gumbeites occurs at the southwestern Berezovsky deposit at the contact with the Shartash pluton. These are quartz veins with molybdoscheelite and tourmaline, which were studied by Kutyukhin (1948). Lower-temperature gumbeites 3–6 including talc-carbonate altered rock (Spiridonov *et al.*, 2000), carbonate-sulfide-quartz veins with scheelite (Shteinberg, 1939; Kurulenko *et al.,* 1984), molybdenite (Kutuykhin, 1937), apatite (Avdonin, 1955), galena, tennantite-tetrahedrite, and sphalerite (Chesnokov *et al.,* 1975), and barren hematite-quartz veins (Spiridoniv *et al.,* 1998$_1$) are found in the other parts of the deposit.

Shartash granodiorite–adamellite complex

Early to Middle Carboniferous gold-bearing granodiorite complexes are located at the eastern slope of the Herzinian Urals (Sobolev, 1966; Bushlyakov and Sobolev, 1976; Ershova and Levitan, 1978; Levitan *et al.*, 1979; Fershtater, 1992; Fershtater *et al.*, 1994; Puchkov, 2010). Usually, this assemblage is regarded to orogenic. This early orogenic, more exactly inversion assemblage, accompanies and terminates the major inversion of folded area that is transition from downwarping to upwarping, termination of arc stage, and transition to orogenic stage. Geochemical and lithological zoning is typical of the granodiorite assemblage of folded areas (Spiridonov, 1995): in troughs (sinclinorium and related structures, at the upper structural level of which, folding basis is usually steep to vertical), there are Na-Ca tonalite-granodiorite-plagiogranite plutons with gold mineralization and negligible Bi content (in the studied area, these are the Upper Iset and similar intrusions); in raises (anticlinorium structures, median masses, microcontinents within folded areas, at the upper level of which folding basis is gentle to horizontal), there are K-Na-Ca granodiorite-adamellite plutons with gold mineralization and high Bi content (in the studied area, these are the Shartash and similar plutons). K-Na-Ca granitic rocks are noticeably enriched in Rb, Pb, and Ba, which are elements coherent to K; these are enriched in F and contain F-rich apatite and biotite (Fershtater *et al.*, 1994; Kholodnov and Bushlyakov, 2002). Formation of the gumbeites is related to the K-Na-Ca plutons (Spiridonov *et al.,* 1997$_2$; 1998$_1$).

The classic Berezovsky deposit of gold-quartz beresite-listvenite formation is located in the distal over-intrusion zone of the Shartash adamellite pluton (Borodaevsky and Borodaevskaya, 1947; Ivanov, 1948; Bellavin *et al.*, 1970; Laipanov and Mikhailova, 1982; Borodaevsky *et al.*, 1984; Sazonov, 1984). The pluton intruded Ordovician to Lower Silurian deformed sedimentary and basaltic sequences cut by dolerites, gabbro, and gabbro-pyroxenites, and hosting plates of serpentinite (Borodaevsky *et al.*, 1984; Rapoport *et al.,* 1994). Serpentinized harzburgite and other ultramafic rocks contain ferrichromite, chrome magnetite, and zincochromite, which are metamorphic products of primary aluminum chromite and magnesiochromite (Spiridonov *et al.*, 1997$_1$, 1998$_1$). Hornfelses of the shallow Shartash pluton contain andalusite and sillimanite. According to N.A. Ershova and R.S. Kurulenko, it comprises three phases of adamellite. Adamellite is cut by numerous veins and dykes of aplite, microadamellite, vein granite including pegmatoids. Adamellite is intruded by dykes of granite-porphyres, diorite-porphyrites, miscrodiorites, and lamprophyres. Dykes of granodiorite-, adamellite-, granite- and plagiogranite-porphyres are predominant. Allanite is typical accessory mineral of these rocks (Spiridonov *et al.*, 2013).

K-Ar age of the Shartash granitoids is 315 ± 15 Ma; K-Ar age of porphyry granite dykes is 316 ± 12 and 306 ± 18 Ma (Ovchinnikov et al., 1989) that is close to the boundary between Early and Middle Carboniferous. Rb/Sr age of the Shartash granitoids and granite-porphyres is 328 ± 18 Ma (Shteinberg *et al.,* 1989); U/Pb age of zircon from the Shartash adamellite and granite-porphyres is 302 ± 3 and 305 ± 7 Ma, respectively (Pribavkin *et al.,* 2012).

Pre-gold quartz-tourmaline metasomatites with Li-bearing muscovite and poor Sn mineralization, K propilite with Mo-Cu mineralization, Na propylite with epidote-quartz veins, talc-carbonate metasomatites, and gumbeites with scheelite are developed within the Berezovsky deposit (Kutyukhin, 1947, 1948; Borodaevsky and Borodaevskaya, 1947; Grabezhev, 1981; Kurulenko *et al.,* 1984; Spiridonov *et al.,* 1998_1, 2000). Quartz-tourmaline metasomatites is related to the Shartash pluton; according to Koptev-Dvornikov (1955), it is referred to the first-stage process. Propylites, gumbeites, and later beresites and listvenites are related to dykes of adamellite-porphyres, microadamellite, diorite-porphyres, and lamprophyres. These are deep-seated dykes or dykes of the second stage according to Koptev-Dvornikov (1955). These dykes terminating the Shartash granodiorite-adamellite complex and altered rocks are paragenetically related to the Shartash pluton (Ershova and Levitan, 1978; Borodaevsky *et al.*, 1984). According to our data, $^{40}Ar/^{39}Ar$ age of muscovite from three samples of the Berezovsky gold-bearing beresite is 306.0 ± 3.6, 312.6 ± 3.8, and 323.6 ± 3.7 Ma (Institute of Geology and Geophysics, Siberian Branch, Russian Academy of Sciences, A.V. Travin analyst). Thus, the isotopic age of post-granitoid metasomatites does not differ from that of the Shartash adamellite and adamellite-porphyres.

Listvenite–like apopicritic gumbeites of the Berezovsky deposit

Studied material. We have studied listvenite-like phlogopite-magnesite metasomatites, a new type of gumbeites developed in the central Berezovsky deposit (level -412 m, Central pit). Its precursor is variolitic picrites occurred as branched subvolcanic dykes of 0.1 to 1.5 m thick cutting foliated hurzburgitic serpentinite. Picrites and serpentinites are cut by dykes of adamellite-porphyres. Varioles range from 3 to 21 mm in size (Fig. 1); chrome spinel is frequent in the core of variole. Hand specimens up to 30 cm across were cut; thin sections, polished sections, and polished samples were prepared. According to optical microscopy, gumbeites replaced deformed picrites.

Analytical techniques. Routine bulk analyses of altered rocks were performed at chemical laboratory at the Institute of Geology of Ore Deposits, Petrography, Mineralogy, and Geochemistry, Russian Academy of Sciences. Content of trace elements was measured by ICP-MS at the Institute of Mineralogy, Geochemistry, and Crystal Chemistry of Rare Elements. Most BSE images and electron microprobe data were obtained with a Jeol SM-6480 LV electron microscope equipped with EDS (N.N. Korotaeva analyst, Division of Petrology, Geological Faculty, Moscow State University). *REE*- and actinide-bearing minerals were examined with a Camebax-microbeam electron microprobe (I.M. Kulikova analyst, Institute of Mineralogy, Geochemistry, and Crystal Chemistry of Rare Elements). R.L. Barinsky in 1958 developed

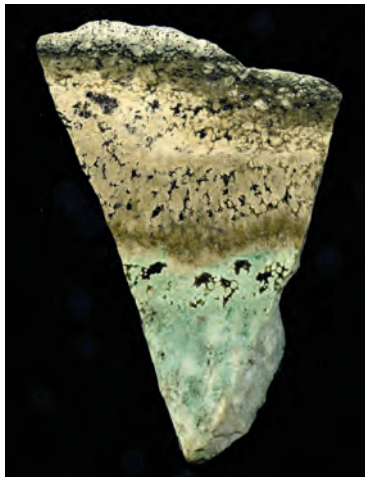

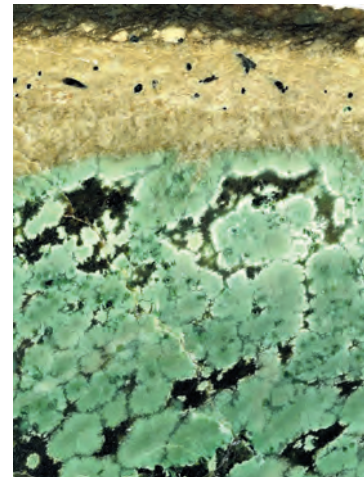

Fig. 1. Fragments of zoned column of apopicritic gumbeites:
(a) white, gray, yellow, and green zones, 168×117 mm;
(b) – gray, yellow, and green zones, 114×82 mm.
Level 512 m, Severny pit, Berezovsky deposit.

Table 1. **Chemical composition of apopicritic gumbeites, Berezovsky deposit (wt.%)**

Component	White-gray zone	Yellow zone	Green zone
SiO_2	43.25	42.64	41.34
TiO_2	1.16	1.07	1.28
P_2O_5	0.27	0.22	0.30
Cr_2O_3	0.25	0.26	0.24
Al_2O_3	6.65	7.69	6.26
Fe_2O_3	3.02	3.44	3.31
MnO	0.24	0.15	0.32
MgO	21.01	20.16	21.93
NiO	0.21	0.17	0.26
CaO	1.84	2.01	2.34
Na_2O	0.30	0.19	0.16
K_2O	3.64	2.99	2.05
CO_2	16.29	16.28	16.52
H_2O^+	1.95	2.30	2.10
S	0.12	0.10	0.02
Total	100.20	99.67	99.43
As, ppm	970	740	170

Notes: Analyses were performed at laboratory of Institute of Geology of Ore Deposits, Mineralogy, Geochemistry, and Petrography, Russian Academy of Sciences; As (ppm) was determined by quantitative spectrometry.

an X-ray technique to determine all *REE* taking into account interference of analytical lines, and effect of selective absorption and excitation of other elements. I.M. Kulikova has improved this technique for modern equipment. Operating conditions are: accelerating voltage 20 kV, current intensity 30 nA, mode of current stabilization. Fourteen *REE*, Y, Th, U, Ca, P, Si, Ti, Al, Fe, Mn, Mg, Sr, Na, Ba, and Ti were measured. The following standards were used: synthetic phosphates of individual *REE* and Y, dioxides of Th, U, and Ti, barite, celestine, and other. Counting time is 10 to 60 s. Analytical lines are measured for two stages: firstly, the relative intensities of even *REE*, Si, Y, Th, P, Ca, and Sr were measured; then the relative intensities of other elements were determined at the same points. The detection limits of *REE* are (wt.%): 0.03 La and Ce, 0.06 Pr, 0.04 Nd, 0.07 Sm, 0.08 Eu, 0.07 Gd, 0.05 Tb, 0.04 Dy, 0.10 Ho, 0.04 Er, 0.07 Tm, 0.04 Yb, and 0.08 Lu. Concentrations of 30 and more elements were calculated with the Calczaf program; ZAF or PAP correction procedure was used. Interlaboratory control attested the reliability of used technique to determine *REE* and actinides.

Metasomatic column. Picrites, precursor rock of gumbeites, contains (n = 8, ppm): 1090 Cr, 1480 Ni, 54 Co (Ni/Co = 27), 34 V, 28 Cu, 115 Zn, 8.2 Pb; this rock is enriched in Ti, P, and *REE* (ppm): 29.5 La, 38.5 Ce, 6.2 Pr, 21.9 Nd, 3.1 Sm, 0.6 Eu, 2.2 Gd, 0.26 Tb, 1.2 Dy, 0.23 Ho, 0.70 Er, 0.11 Tm, 0.26 Yb, 0.15 Lu, 6.5 Y, 178 Zr, 6.8 Hf, 47 Nb, 13.4 U, 11.6 Th, *LREE/HREE* = 17, Th/U = 0.9 (ISP-MS, N.V. Vasil'ev and L.P. Yurchenkova analysts, Institute of Mineralogy, Geochemistry, and Crystal Chemistry of Rare Elements). Content of Cr, Ni, Co, V, Cu, and Zn is typical of picrite; concentration of Zr, Nb, Hf, *REE*, and actinides is typical of alkali picrite.

The chemical composition of gumbeites from various zones of the metasomatites column (Fig. 1) is given in Table 1. Chemical variations are not great. Strong predominance of Mg over Fe and Ca characteristic of picrite retains in altered rocks. Content of Ca decreases to the inner zone, whereas that of Na, S, and As noticeably increases (Table 1).

Apopicritic gumbeites is composed of Mn-poor magnesite, F-rich phlogopite, quartz, potassium feldspar, albite, chlorite, F-rich muscovite and phengite, tourmaline (dravite), rutile (after ilmenite), to less extent dolomite, fluorapatite, monazite-(Ce), zircon, xenotime, gersdorffite, siegenite, millerite, Co-bearing pyrite, and galena. Talc-magnesite metasomatic rock with hematite, and accessory hydroxylphlogopite, hydroxylapatite, and violarite occurs in the outer zone of the column.

White inner zone of the apopicritic gumbeites column up to 2 cm in thickness (Fig. 1a) contacting with gumbeitized porphyry granodiorite or potassium feldspar-carbonate-quartz vein is composed of varigranular aggregates of magnesite, quartz and F-rich phlogopite (Fig. 2); the proportion of minerals is strongly variable from place to place; structure is massive, in some cases, it is directive, where gumbeites replaced bands of deformed picrite. Next gray zone up to 2 cm thick is composed of abundant phlogopite, quartz, and magnesite (Fig. 3) with inclusions of rare large crystals of albite and clusters of albite and potassium feldspar (Fig. 1b). Mega- and microscopically, in white and gray zones, features of primary

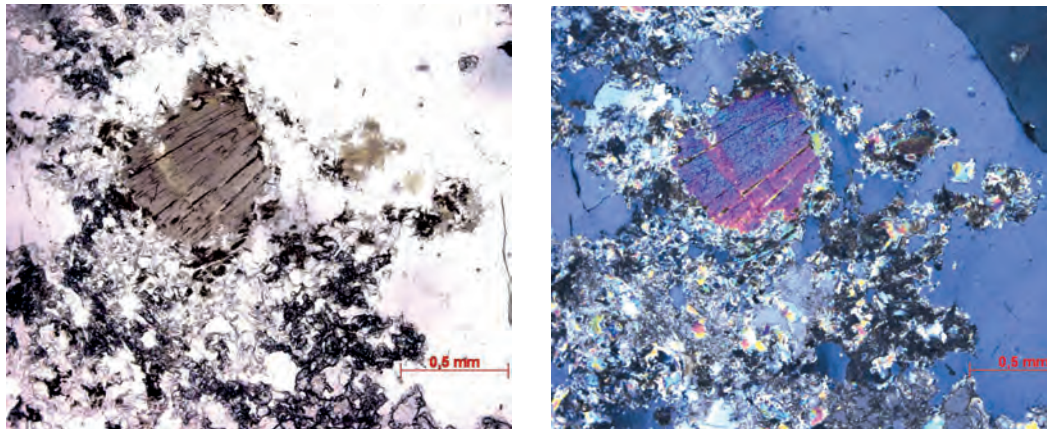

Fig. 2. Photomicrographs of white zone of apopicritic gumbeites column. Magnesite-phlogopite-quartz gumbeites. (a) Normal light, (b) crossed polars.

Fig. 3. Photomicrographs of gray zone of apopicritic gumbeites column. Quartz-magnesite-phlogopite gumbeites. (a) Normal light, (b) crossed polars.

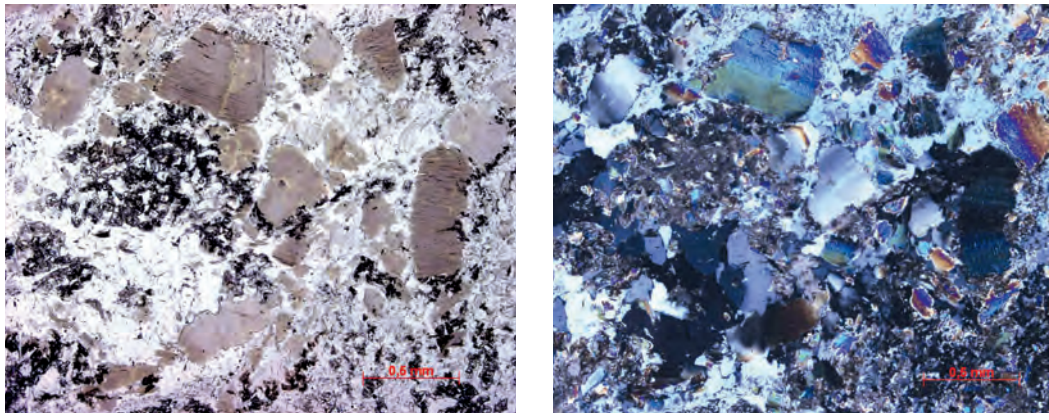

picrite are absent; chrome spinel and ilmenite are completely dissolved. Next yellow zone ranging from 3 to 11 cm in thickness contains tourmaline and dolomite along with magnesite and does not contain green chlorite and Cr-bearing muscovite. Next green zone of 15 to 25 cm thick contains pods of green chlorite and relict chrome spinel in aggregates of Cr-bearing muscovite and phengite (Figs. 1, 4). The outer zone comprises talc-magnesite metasomatic rock with hematite; the structure is massive as usual and foliated with predominant orientation of hematite plates; crystals of dark gray magnesite are not deformed (pre-gumbeites foliation). Boundaries between zones are clear. The size of crystals of magnesite ranges from 0.0*n* to 10 – 14 mm; that of quartz, potassium feldspar and albite, and phlogopite reaches 3, 4, and 2 mm, respectively. The minerals are irregularly distributed frequently composing pockets.

Gumbeites of the yellow, gray, and white zones are enriched in Ba (average 1138 ppm, occasionally up to 3800 ppm), Rb (average 219 ppm), contains Sr (average 123 ppm), Cs (average 2.99 ppm), Ag (average 437 ppb), and Au (7.0 ppb). Thus, gumbeitization resulted in strong accumulation of Ba and Rb coherent to K and Ag, but not Au.

Relict minerals. Zincochromite is partially retained in the green zone of apopicritic gumbeites (Fig. 2). The grain size is up to 2 mm. The Ti-free, Al- and Mg-poor mineral compositionally corresponds to the formula $(Zn_{0.7-0.8}Fe^{2+}_{0.2-0.3})_1(Cr_{1.3-1.4}Fe^{3+}_{0.4-0.6}Al_{0.1-0.2})_2O_4$ ((Table 2). Spinels of similar morphology and composition occur in picrite and peridotitic serpentinite beyond gumbeites aureoles. Both zinc chromite and other spinels are the products of regional submergence metamorphism with high-alkali and high-oxidative fluids; when

ultramaphic and mafic rocks are metamorphosed together, Zn from mafic rocks compensates deficiency of Fe^{2+} in spinels (Spiridonov *et al.*, 1997_1; 1998_2). Spinel is brecciated and significantly replaced by Cr-rich muscovite, phengite, and phlogopite.

Picrite in inter-variole places contained mumerous plates of ilmenite up to 2.5 × 2.5 × 0.5 mm in size. Pseudomorphs of long-prismatic rutile after deformed, curved, and twisted plates of ilmenite are abundant in the green and yellow zones of gumbeites column.

Quartz, one of the major minerals of white and gray zones, is abundant in the yellow and green zones. Its grains range from 0.0*n* to 3 mm in size. Megascopally, the mineral is light gray, opaque. It contains numerous tiny fluid inclusions with liquid CO_2. Quartz is close intergrown with phlogopite, magnesite, and potassium feldspar.

Carbonates are the major constituents of apopicritic gumbeites. Magnesite is predominant in all zones of the column. Megascopally, magnesite is black in talc-magnesite metasomatic rock of the outer zone; this mineral is white to light yellow in phlogopite-quartz-magnesite inner zone. The grains of the mineral ranges from 0.0*n* to 14 mm. Aggregates of magnesite are sufficiently abundant. The core of such aggregates is unzoned single rhombohedron rimmed by small zoned rhombohedra of Fe-rich magnesite. Magnesite is Mn-poor in all zones of the metasomatic column. The Fe/(Fe + Mg) value of the mineral from talc-magnesite rock of the outer zone ranges from 0.06 to 0.12. Magnesite from the green zone contains traced Ca and Mn, and up to 0.3 wt.% Zn; its Fe/(Fe + Mg) value is 0.13 to 0.16 (Table 3). Magnesite from the yellow zone contains traced Ca and Mn; its Fe/(Fe + Mg) value is 0.09 to 0.16 (Table 4).

Small pockets of late dolomite occur in the aggregates of magnesite of the yellow zone. In addition, dolomite heals fractures in deformed crystals of tourmaline (Fig. 5). The composition of dolomite corresponds to the formula $Ca_{0.98\text{-}1}Mg_{0.83\text{-}0.92}Fe_{0.09\text{-}0.15}Mn_{0\text{-}0.02}(CO_3)_2$.

Phlogopite, one of the major minerals of white and gray zones, occurs as lamellar and columnar crystals up to 1 to 2 mm in size. Split fan-shaped crystals of phlogopite enclosed in quartz are frequent in the white zone. Microscopically, phlogopite is light brown to brown, unzoned as usual (Figs. 3, 4). Phlogopite is F-bearing, Ti-poor and contains ca. 0.5 wt.% Cr.

Table 2. **Chemical composition (wt.%) of relict zincochromite from apopicritic phlogopite-magnesite gumbeites, Berezovsky deposit**

Component	1	2	3	4	5	6	7	8	9	10
ZnO	27.46	27.01	26.26	26.54	26.68	26.26	26.41	26.04	26.01	25.52
FeO	6.48	6.89	6.68	6.48	7.47	6.98	7.28	7.32	7.00	8.39
MgO	0.30	0.32	0.46	0.62	0.30	0.55	0.28	0.62	0.81	0.56
NiO	0.34	0.19	0.26	0.28	0.22	0.49	0.25	0.19	bdl	bdl
MnO	bdl	bdl	bdl	bdl	bdl	bdl	0.43	bdl	0.37	bdl
Cr_2O_3	43.25	43.10	42.14	41.83	44.12	41.99	43.02	41.44	46.08	46.36
Fe_2O_3	18.53	18.12	18.33	19.46	19.07	20.65	19.85	20.89	13.31	13.32
Al_2O_3	3.89	4.15	3.88	3.91	3.34	3.67	3.58	4.02	5.74	5.68
Total	100.34	99.78	98.01	99.12	101.20	100.69	101.10	99.92	99.32	99.83
Atoms per formula unit										
Zn	0.77	0.76	0.75	0.75	0.74	0.73	0.73	0.73	0.72	0.71
Fe^{2+}	0.20	0.22	0.22	0.21	0.24	0.22	0.23	0.23	0.22	0.26
Mg	0.02	0.015	0.02	0.03	0.015	0.03	0.015	0.035	0.05	0.03
Ni	0.01	0.005	0.01	0.01	0.005	0.02	0.01	0.005	–	–
Mn	–	–	–	–	–	–	0.015	–	0,01	–
Total	1									
Cr	1.29	1.30	1.29	1.26	1.31	1.25	1.28	1.24	1.37	1.37
Fe^{3+}	0.53	0.52	0.53	0.56	0.54	0.59	0.56	0.58	0.38	0.38
Al	0.18	0.18	0.18	0.18	0.15	0.16	0.16	0.18	0.25	0.25
Total	2									

Notes. A Jeol SM-6480 LV electron microprobe, N.N. Korotaeva analyst. Content of Ti and Si is below detection limit, FeO and Fe_2O_3 are calculated by stoichiometry. Here and below bdl is below detection limit.

Table 3. **Chemical composition (wt.%) of magnesite from green zone of apopicritic phlogopite-magnesite gumbeites, Berezovsky deposit**

Component	11	12	13	14	15	16	17	18	19	20
MgO	38.65	38.42	37.69	37.32	37.72	37.13	36.76	37.04	36.73	36.25
FeO	10.51	11.19	11.51	11.75	12.42	12.46	12.57	12.61	12.95	13.47
ZnO	0.18	0.17	bdl	0.19	0.24	0.23	0.19	0.25	0.31	0.21
MnO	0.10	0.12	bdl	0.12	0.13	0.13	0.14	0.08	0.11	0.17
CaO	0.10	0.12	bdl	0.10	bdl	0.09	0.15	0.09	0.10	0.14
SrO	bdl	bdl	bdl	0.10	bdl	bdl	bdl	bdl	0.09	bdl
Total	49.54	50.00	49.20	49.57	50.51	50.03	49.80	50.07	50.29	50.25
Atoms per formula unit										
Mg	0.87	0.86	0.85	0.85	0.84	0.84	0.84	0.84	0.84	0.83
Fe	0.13	0.14	0.15	0.15	0.16	0.16	0.16	0.16	0.16	0.17
Total	1									

Notes. A Jeol SM-6480 LV electron microprobe, N.N. Korotaeva analyst.

Table 4. **Chemical composition (wt.%) of magnesite from yellow zone of apopicritic phlogopite-magnesite gumbeites, Berezovsky deposit**

Component	21	22	23	24	25	26	27	28	29
MgO	41.51	41.06	38.40	38.86	37.87	38.41	38.40	37.64	37.86
FeO	6.91	8.10	9.99	11.20	11.30	11.34	11.56	12.46	12.70
MnO	0.16	0.13	0.16	0.12	0.12	0.13	0.13	0.28	0.13
CaO	bdl	bdl	0.17	0.11	bdl	0.08	0.17	0.16	0.15
SrO	bdl	bdl	bdl	bdl	0.10	bdl	bdl	bdl	0.10
Total	48.58	49.28	48.72	50.28	49.39	49.96	50.27	50.55	50.94
Atoms per formula unit									
Mg	0.91	0.90	0.87	0.86	0.86	0.86	0.86	0.84	0.84
Fe	0.09	0.10	0.13	0.14	0.14	0.14	0.14	0.16	0.16
Total	1								

Notes. A Jeol SM-6480 LV electron microprobe, N.N. Korotaeva analyst.

Phlogopite is frequently replaced by colorless Fe-poor chlorite or muscovite.

Potassium feldspar is abundant in gray, yellow, and green zones. Microcline without grid pattern occurs as separate grains in matrix of magnesite and quartz (± micas) and as clusters with albite. Potassium feldspar contains traces of Ca, up to 2% Ba, 3−60% of albite end-member, and 0−4% of hyalophane end-member (Table 5). Positive correlation between Ba and Na substituting K was established in the mineral.

Albite is relatively common in the gumbeites described; it is abundant in the gray zone, where albite and potassium feldspar occur as occasionally split composite crystals up to 3 mm. Crystals display predominantly albite twinning. The chemical composition of albite is as follows (anal. 38, wt.%): SiO_2 68.26; Al_2O_3 19.60; CaO 0.20; Na_2O 11.46; K_2O 0.10; total is 99.62 (N.N. Korotaeva analyst); formula is $(Na_{0.975}Ca_{0.01}K_{0.005})_{0.99}[Al_{1.01}Si_3O_8]$, or $Na_{98.5}Ca_1K_{0.5}$.

White micas. Flour-bearing (1−2.5 wt.% F) white micas are abundant in the gray and green zones of the apopicritic gumbeites column. The Cr-richest micas occur as replacement rims around zincochromite (Fig. 2; Table 5, anal. 39−44); Cr-poor micas (Table 6, anal. 45, 46) are disseminated in quartz-potassium feldspar-phlogopite-magnesite matrix. In these micas, Cr for Al chemical substitution is pronounced. Muscovite and muscovite-phengite enriched in Cr are extremely enriched in Mg. The composition of the Mg-richest F-bearing muscovite (Table 6, anal. 43) is specific; it is close to $KAlMg[(OH_{0.5}F_{0.5})_1/AlSi_3O_{10}]$. Potassium is predominant in micas; deficiency at the K site is insignificant.

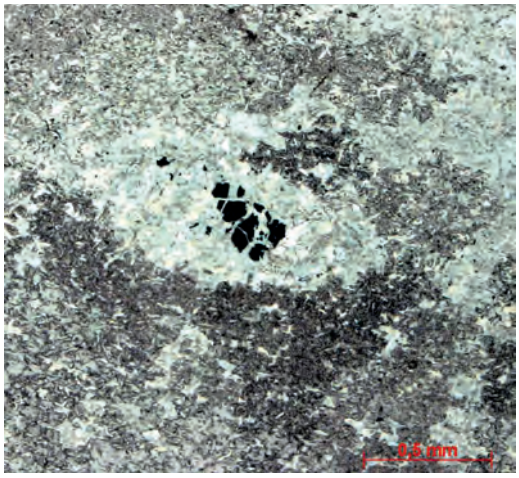

Fig. 4. Photomicrograph of green zone of apopicritic gumbeites column. Relict zincochromite (black) in aggregate of Cr-rich muscovite. Groundmass is composed of Fe-rich magnesite, muscovite, phlogopite, quartz, and potassium feldspar. Normal light.

Fig. 5. Photomicrographs of long prismatic zoned crystal of dravite in phlogopite-magnesite matrix. Crystal is deformed; parting fractures are filled by dolomite. (a) Normal light, (b) crossed polars.

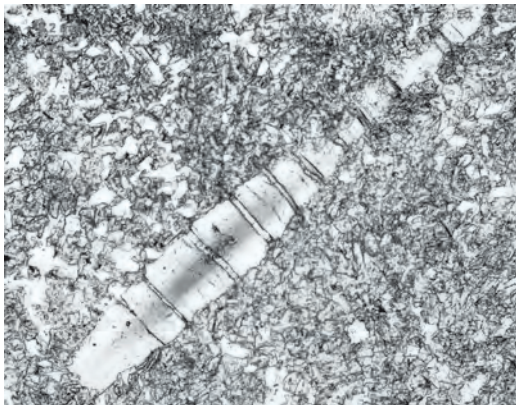

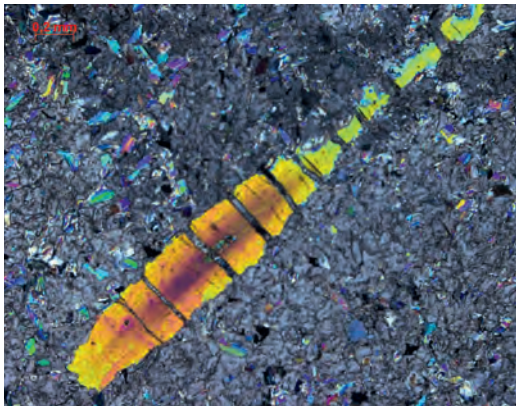

F-bearing muscovite, muscovite-phengite, and phengite with noticeable content of Ti with overgrowth rims of muscovite enriched in Ba and Na are developed in the yellow zone; their compositions are given in Table 7. Ti is concentrated in muscovite and phengite, whereas Ba and Na are concentrated in low-Si muscovite.

Rutile occurs as aggregate-type pseudomorphs after plates of ilmenite (Figs. 6, 7). The composition of rutile is as follows (anal. 54, wt.%): TiO_2 98.52, Fe_2O_3 0.51, WO_3 0.13, ThO_2 0.01; total is 99.17 (I.M. Kulikova, analyst); Y, Ce, La, Nd, U, Ca, and Zr are below detection limits.

Tourmaline (dravite). Short prismatic metacrystals of tourmaline up to 4 mm in length (Fig. 5) are common in the yellow zone. The crystals are poorly zoned. Cores of some crystals are brownish green in transmit light with the Fe/(Fe + Mg) value 0.18 – 0.20; rims of these crystals are greenish and yellowish-greenish with the lower Fe/(Fe + Mg) value 0.10 – 0.16. In other crystals the zoning is reversal. Tourmaline of picritic gumbeites is Cr-free, and Ti-, Fe^{2+}, and Fe^{3+}-poor dravite (Table 8). The remarkable deficiency of Na (up to 22%) indicates high acidity of hydrothermal fluid. The composition of tourmaline corresponds to the formula $(Na_{0.8\text{-}0.9}Ca_{0\text{-}0.1}\square_{0.1\text{-}0.2})_1(Mg_{2.3\text{-}2.5}Fe^{2+}_{0.3\text{-}0.6}Fe^{3+}_{0\text{-}0.1}Al_{0\text{-}0.3})_3Al_6(BO_3)_3[(Si_{5.9\text{-}6}Al_{0\text{-}0.1})_6O_{18}](OH_{3.8\text{-}4}O_{0\text{-}0.2})_4$, value 0.10-0.20, average 0.16.

Microscopically, dravite with relict lamellae of ilmenite is green-brown to brown and contains up to 5 wt.%, up 1.5 wt.% Ti, and inclusions of acicular rutile.

Fluorapatite is abundant mineral. Clusters and aggregates of apatite grains are frequently confined to the aggregate pseudomorphs of acicular rutile after deformed plates of ilmenite (Fig. 6, 7). The size of crystals of fluorapatite is up to 0.5 mm. It forms compromise growth surface with rutile, quartz, magnesite, and potassium feldspar. The chemical composition of fluorapatite is given in Table 9 (anal. 63 – 71). The separate measurement (no. 72) with determination of *REE* was performed by I.M. Kulikova; this composition is as follows (wt.%): CaO 56.06; SrO 0.24; Na_2O 0.05; Y_2O_3 0.09; Ce_2O_3 0.07; Nd_2O_3 0.13; FeO 0.05; MnO 0.06; UO_2 0.01; P_2O_5 42.01; SiO_2 0.44; SO_3 0.28; F 3.67, total is ($-O = F_2$) 101.61; Cl, La, Pr, Sm, Eu, Gd, Tb, Dy, Ho, Er, Tm, Yb, Lu, Th are below detection limits. Formula of this apatite is $(Ca_{4.97}Sr_{0.01}Na_{0.01}Y_{0.01})_5(P_{2.94}Si_{0.04}S_{0.02})_3O_{12}F_{0.96}$. This is all-fluorine apatite. Phosphorous in the gumbeites apatite is substituted to some extent with Si and S that testifies to the high temperature of formation and high oxidation potential (Peng *et al.*, 1997; Phosphates.., 2003).

Table 5. **Chemical composition (wt.%) of potassium feldspar from apopicritic phlogopite-magnesite gumbeites, Berezovsky deposit**

Component	30	31	32	33	34	35	36	37
SiO_2	65.27	64.71	64.49	64.54	64.07	64.57	63.61	63.65
Al_2O_3	18.62	18.59	18.50	18.53	18.57	18.77	18.84	18.89
Fe_2O_3	bdl	bdl	bdl	bdl	bdl	0.15	bdl	bdl
CaO	bdl	bdl	bdl	bdl	0.11	bdl	bdl	0.16
Na_2O	0.40	0.37	0.52	0.65	0.73	0.45	0.74	0.71
K_2O	16.32	16.25	16.00	15.73	15.64	15.90	15.30	15.18
BaO	0.23	0.34	0.47	0.66	0.67	1.22	2.19	2.29
Total	100.85	100.27	99.98	100.10	99.78	101.06	100.68	100.88
				Atoms per formula unit				
K	0.96	0.96	0.94	0.93	0.93	0.94	0.90	0.90
Na	0.04	0.03	0.05	0.06	0.06	0.04	0.06	0.06
Ba	-	0.01	0.01	0.01	0.01	0.02	0.04	0.04
Total				1				
Si	3.00	2.99	2.99	2.99	2.97	2.98	2.96	2.96
Al	1.00	1.01	1.01	1.01	1.03	1.01	1.04	1.04
Fe^{3+}	–	–	–	–	–	0.01	–	–
Total				4				

Notes. A Jeol SM-6480 LV electron microprobe, N.N. Korotaeva analyst.

Table 6. **Chemical composition (wt.%) of Cr-bearing muscovite (39-45) and phengite (46) from apopicritic phlogopite-magnesite gumbeites, Berezovsky deposit**

Component	39	40	41	42	43	44	45	46
SiO_2	48.16	47.60	47.54	47.27	46.61	47.47	49.40	49.61
Al_2O_3	26.38	26.65	25.13	26.11	24.96	26.67	30.83	29.43
Cr_2O_3	2.98	2.68	2.58	2.36	2.16	1.47	0.41	0.39
Fe_2O_3	1.26	1.58	1.13	1.76	1.82	1.19	0.27	0.36
MgO	5.52	3.99	7.10	5.57	8.71	6.19	3.66	3.85
Na_2O	0.18	0.12	0.15	0.17	0.25	0.18	0.21	0.22
K_2O	11.14	10.91	10.98	10.97	10.89	11.06	11.12	11.12
F	1.69	0.98	1.87	1.88	2.32	1.93	1.37	1.10
H_2O^+	5.14	6.66	4.36	4.94	2.43	4.68	6.75	7.05
Total $-O = F_2$	101.74	100.76	100.05	100.24	99.17	100.03	103.44	102.67
				Atoms per formula unit				
K	0.93	0.95	0.94	0.94	0.91	0.94	0.93	0.94
Na	0.02	0.02	0.02	0.02	0.03	0.02	0.03	0.03
□	0.05	0.03	0.04	0.04	0.06	0.04	0.04	0.03
Total				1				
Al	1.24	1.38	1.11	1.23	0.96	1.25	1.61	1.59
Cr	0.16	0.14	0.13	0.13	0.11	0.08	0.02	0.02
Fe^{3+}	0.06	0.08	0.06	0.08	0.09	0.06	0.02	0.01
Mg	0.54	0.40	0.70	0.56	0.84	0.61	0.35	0.38
Total				2				
Si	3.18	3.24	3.15	3.17	3.04	3.16	3.23	3.29
Al	0.82	0.76	0.85	0.83	0.96	0.84	0.77	0.71
Total				4				
OH	1.20	1.60	1.02	1.17	0.56	1.10	1.56	1.65
F	0.39	0.21	0.39	0.40	0.48	0.41	0.28	0.23
Total	1.59	1.81	1.41	1.57	1.14	1.51	1.84	1.85

Notes. A Jeol SM-6480 LV electron microprobe, N.N. Korotaeva analyst. Contents of Ca, Mn, and Ti are below detection limits. H_2O^+ calculated by stoichiometry.

Table 7. **Chemical composition (wt.%) of muscovite (48, 50, 51), phengite (47, 49), Ba-bearing muscovite (52, 53) from yellow zone of apopicritic phlogopite-magnesite gumbeites, Berezovsky deposit**

Component	47	48	49	50	51	52	53
SiO_2	48.84	48.84	49.95	48.05	47.92	46.04	46.18
TiO_2	0.95	0.77	0.66	0.27	0.13	bdl	bdl
Al_2O_3	28.44	29.04	29.11	29.53	30.21	32.90	32.82
Fe_2O_3	1.53	1.53	0.47	1.29	2.18	1.81	1.38
MgO	3.74	4.07	4.51	4.89	4.12	2.72	2.80
Na_2O	0.17	0.19	0.19	0.20	0.21	0.41	0.35
K_2O	11.09	11.18	11.18	11.23	11.18	10.63	10.44
BaO	bdl	bdl	bdl	bdl	bdl	1.47	1.71
F	1.27	1.30	1.00	1.29	0.89	0.93	1.05
H_2O^+	6.94	6.64	6.76	5.99	6.81	6.89	6.80
Total − O = F_2	102.44	103.01	103.41	102.23	103.27	103.41	103.19
			Atoms per formula unit				
K	0.95	0.94	0.93	0.94	0.94	0.90	0.89
Na	0.02	0.02	0.02	0.03	0.03	0.05	0.05
Ba	–	–	–	–	–	0.04	0.04
□	0.03	0.04	0.05	0.03	0.03	0.01	0.02
Total				1			
Al	1.50	1.48	1.50	1.45	1.48	1.64	1.65
Fe^{3+}	0.08	0.08	0.03	0.06	0.11	0.09	0.07
Ti	0.05	0.04	0.02	0.01	0.01	–	–
Mg	0.37	0.40	0.45	0.48	0.40	0.27	0.28
Total				2			
Si	3.26	3.22	3.26	3.16	3.15	3.06	3.08
Al	0.74	0.78	0.74	0.84	0.85	0.94	0.92
Total				4			
OH	1.64	1.55	1.58	1.39	1.58	1.62	1.60
F	0.27	0.27	0.21	0.27	0.18	0.20	0.22
Total	1.91	1.82	1.79	1.66	1.76	1.82	1.82

Notes. A Jeol SM-6480 LV electron microprobe, N.N. Korotaeva analyst. Contents of Cr, Ca, and Mn are below detection limits. H_2O^+ calculated by stoichiometry.

Fig. 6. Back-scattered electron image of grains of fluorapatite (light gray) confined to aggregate pseudomorph of acicular rutile after plates of ilmenite. Small bright white crtstal are monazite. Groundmass is composed of cluster of magnesite, quartz, phlogopite, potassium feldspar, and muscovite.

Fig. 7. Back-scattered electron image of fluorapatite (light gray) intergrown with rutile (white) in aggregate of magnesite, phlogopite, and muscovite.

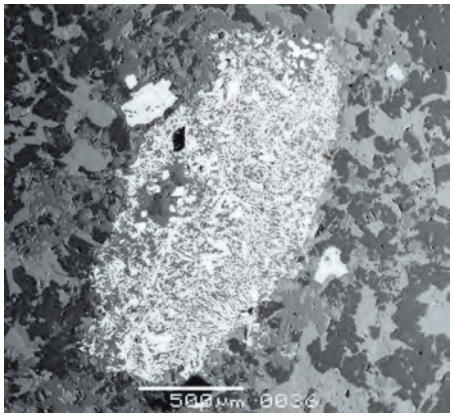

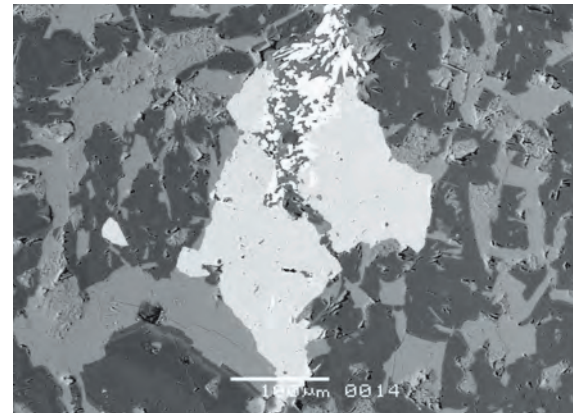

Table 8. **Chemical composition (wt.%) of tourmaline (dravite) from apopicritic phlogopite-magnesite gumbeites, Berezovsky deposit**

Component	55	56	57	58	59	60	61	62
SiO_2	37.01	36.61	37.18	37.00	36.61	36.76	36.94	36.96
TiO_2	bdl	0.11	0.26	0.33	0.17	0.28	bdl	0.10
Al_2O_3	32.78	31.25	31.61	31.82	31.72	32.21	33.75	33.29
Fe_2O_3		0.42	0.07		0.57			
FeO	2.11	3.64	4.20	3.93	3.94	3.76	1.95	3.18
MgO	10.13	9.81	9.96	9.91	9.83	9.83	9.68	9.60
CaO	0.13	0.24	0.15	0.48	0.10	0.44	0.10	0.17
Na_2O	2.41	2.51	2.84	2.59	2.85	2.73	2.56	2.62
K_2O	bdl	bdl	bdl	bdl	0.10	bdl	bdl	bdl
Total	84.58	84.59	86.28	86.05	85.88	86.00	84.98	85.92
				Atoms per formula unit				
Na	0.76	0.80	0.89	0.81	0.90	0.85	0.80	0.82
K	–	–	–	–	0.02	–	–	–
Ca	0.02	0.04	0.03	0.08	0.02	0.08	0.02	0.03
□	0.22	0.16	0.08	0.11	0.06	0.07	0.18	0.15
Total				1				
Al	0.27	0.04	–	0.04	–	0.09	0.40	0.26
Fe^{3+}	–	0.05	0.01	–	0.07	–	–	–
Ti	–	0.01	0.03	0.04	0.02	0.03	–	0.01
Fe^{2+}	0.28	0.50	0.57	0.53	0.53	0.51	0.27	0.43
Mg	2.45	2.40	2.39	2.39	2.38	2.37	2.33	2.30
Total				3				
Al	6.00	6.00	6.00	6.00	6.00	6.00	6.00	6.00
Total				6				
Al	–	–	0.01	0.02	0.06	0.05	0.03	0.05
Si	6.00	6.00	5.99	5.98	5.94	5.95	5.97	5.95
Total				6				
O	0.07	–	–	0.08	–	0.11	0.21	0.10
OH	3.93	4.00	4.00	3.92	4.00	3.89	3.79	3.90
Total				4				

Notes. A Jeol SM-6480 LV electron microprobe, N.N. Korotaeva analyst. Contents of Cr and Mn are below detection limits.

Zircon is a member of solid solution series $Zr[SiO_4]$ (zircon proper) – $Hf[SiO_4]$ (gaphnon) – $Th[SiO_4]$ (thorite) – $U[SiO_4]$ (coffinite) – $Y[PO_4]$ (xenotime) (Heinrich, 1962; Krasnobaev, 1986; Frondel and Collette, 1957; Gratz and Heinrich, 1997; Strunz and Nickel, 2001; Zircon..., 2004; Förster, 2006). Accessory zircon is typical of magmatic rocks from granites, granitic pegmatites, rhyolite to gabbros and basalts; baddeleite is formed instead of zircon in magmatic rocks undersaturated in silica. A lot of publications are devoted to morphology and composition of zircon from magmatic rocks (and weathered products); there is a rather complete review (Zircon.., 2004) and reviews for the Urals (Krasnobaev, 1986; Votyakov *et al.,* 2011). As a result of magmatic fractionation, Hf, U, and Th are accumulated in zircon and high-tempreature zircon is enriched in the xenotime end-member. Zirconium is established to be mobile in alkali high-temperature hydrothermal solutions; high-temperature altered rock enriched in newly formed zircon was found (albitite – mariupolite) (Frondel and Collette, 1957; Rubin *et al.,* 1993; Zircon..., 2004).

Zircon in phlogopite-magnesite gumbeites occurs as disseminated prismatic and short-prismatic crystals up to 90 μm in length, which are frequently associated with fluorapatite (Figs. 8–10). Compromise growth surfaces are frequent between zircon, quartz, magnesite, and fluorapatite. The predominant zones of zircon crystals contain (wt.%): 1.4–1.9 Hf, 0.6–1.2 P_2O_5, traces of U, Th, and Y; the zones enriched in U contain up to 3.8 wt.% U, 2.4 Hf, 1.4 Y, 0.8 Th (Table 10). Zircon from gumbeites contains 1–2% of hafnon end-member, 0–3% of coffinite end-member, 0–1% of thorite end-member, and 0–3% of xenotime end-member.

Table 9. **Chemical composition (wt.%) of fluorapatite from apopicritic phlogopite-magnesite gumbeites, Berezovsky deposit**

Component	63	64	65	66	67	68	69	70	71
CaO	54.06	54.40	54.70	54.79	54.83	54.94	54.56	55.04	55.31
SrO	0.94	bdl	bdl	bdl	bdl	bdl	bdl	bdl	bdl
Ce_2O_3	bdl	0.25	bdl	bdl	bdl	bdl	bdl	bdl	bdl
FeO	0.14	0.21	0.19	bdl	bdl	bdl	bdl	bdl	bdl
MnO	bdl	bdl	0.15	bdl	bdl	bdl	bdl	bdl	bdl
P_2O_5	41.47	41.23	41.19	41.38	40.89	41.29	40.61	40.83	42.18
SiO_2	0.30	0.36	0.36	0.43	0.45	0.46	0.46	0.53	0.58
SO_3	bdl	0.30	0.11	bdl	0.29	0.10	0.45	bdl	bdl
F	3.98	3.32	3.46	3.30	3.49	3.35	3.59	3.24	3.18
Total $- O=F_2$	99.21	98.67	100.05	99.57	98.88	99.61	98.94	99.25	99.91
Atoms per formula unit									
Ca	4.94	4.98	4.98	5.00	5.00	5.00	5.00	5.00	5.00
Sr	0.05	–	–	–	–	–	–	–	–
Ce	–	0.01	–	–	–	–	–	–	–
Fe	0.01	0.01	0.01	–	–	–	–	–	–
Mn	–	–	0.01	–	–	–	–	–	–
Total					5				
P	0.97	0.95	0.96	0.96	0.94	0.96	0.93	0.96	0.95
Si	0.03	0.03	0.03	0.04	0.04	0.03	0.04	0.04	0.05
S	–	0.02	0.01	–	0.02	0.01	0.03	–	–
Total					1				
F	1.08	0.90	0.93	0.89	0.94	0.90	0.97	0.87	0.85

Notes. A Jeol SM-6480 LV electron microprobe, N.N. Korotaeva analyst.

Fig. 8. Back-scattered electron image of fluorapatite (light) intergrown with zircon (white) in matrix of magnesite (dark gray), phlogopite, potassium feldspar, muscovite (light gray), and quartz (gray).

Fig. 9. Back-scattered electron image of cluster of zircon crystals (white), two of which are large. Groundmass is composed of intergrown magnesite (dark gray), quartz (gray), phlogopite, potassium feldspar, and muscovite (light gray).

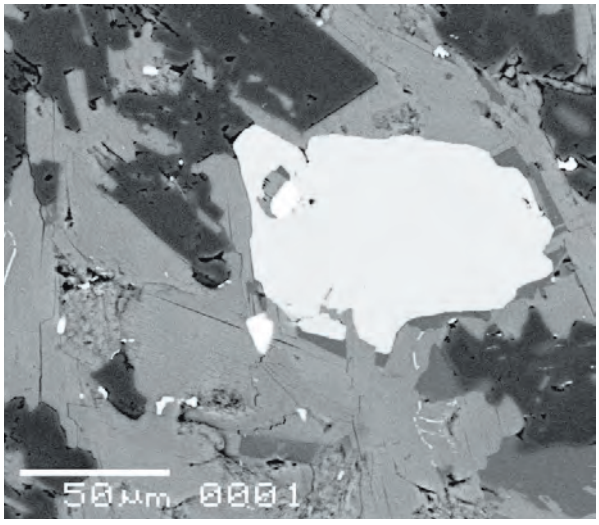

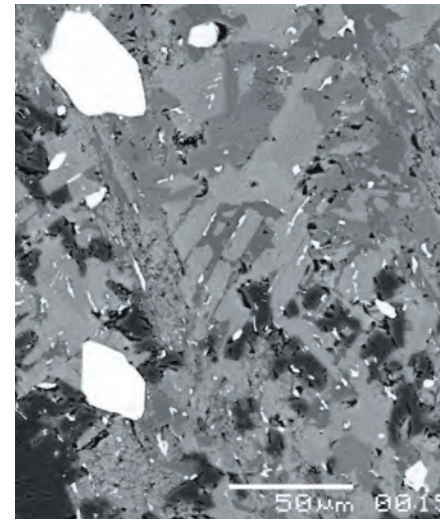

Table 10. **Chemical composition (wt.%) of zircon from apopicritic phlogopite-magnesite gumbeites, Berezovsky deposit**

Component	73	74	75	76	77	78	79	80
ZrO_2	65.93	65.71	64.93	63.63	63.51	63.66	63.29	60.34
HfO_2	1.63	1.92	1.45	1.39	1.40	2.41	1.99	2.02
UO_2	0.01	0.02	0.01	0.02	0.03	0.59	2.19	3.88
ThO_2	bdl	bdl	bdl	0.65	0.48	0.20	0.80	0.60
Y_2O_3	bdl	bdl	0.66	1.35	1.09	0.23	0.74	0.90
Ce_2O_3	bdl	bdl	0.11	bdl	0.37	bdl	bdl	bdl
Nd_2O_3	0.05	0.06	0.05	0.15	0.20	bdl	bdl	bdl
Gd_2O_3	0.07	bdl	bdl	bdl	bdl	bdl	bdl	bdl
Yb_2O_3	bdl	bdl	bdl	bdl	bdl	bdl	bdl	0.05
SiO_2	32.38	32.19	32.32	31.39	31.15	32.03	32.07	31.07
P_2O_5	0.13	0.15	0.58	1.06	1.14	0.14	0.48	0.64
Total	100.20	100.05	100.01	99.64	99.38	99.26	101.56	99.50
				Atoms per formula unit				
Zr	0.99	0.99	0.98	0.96	0.96	0.97	0.95	0.93
Hf	0.01	0.02	0.01	0.01	0.01	0.02	0.02	0.02
U	–	–	–	–	–	0.01	0.02	0.03
Th	–	–	–	0.01	–	–	–	–
Y	–	–	0.01	0.02	0.02	–	0.01	0.02
Ce	–	–	–	–	0.01	–	–	–
Si	1.00	0.99	0.99	0.97	0.97	1.00	0.99	0.98
P	–	–	0.01	0.03	0.03	–	0.01	0.02

Notes. A Camebax-microbeam electron microprobe, I.M. Kulikova analyst. Contents of S, La, Pr, Sm, Er, Dy, Ho, Tm, and Lu are below detection limits.

Fig. 10. Back-scattered electron image of complexly zoned crystal of zircon. Points correspond to numbers in Table 10.

Fig. 11. Back-scattered electron image of aggregate pseudomorph of long-prismatic crystals of rutile after deformed and partly brecciated large plate crystal of ilmenite. The most deformed places are dissolved; pockets of crystals of monazite (white) are developed instead of them. Groundmass is composed of intergrown magnesite (dark gray), quartz (gray), potassium feldspar, and micas. Long fluorapatite (light gray) is above lamella.

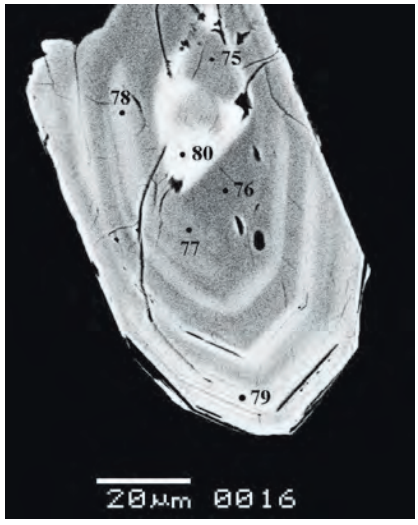

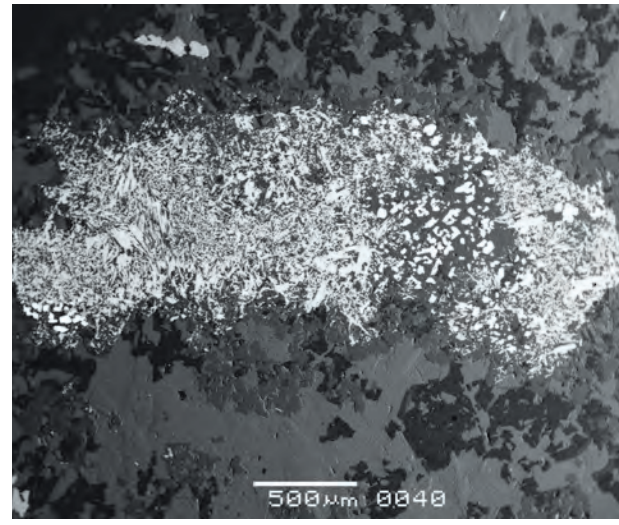

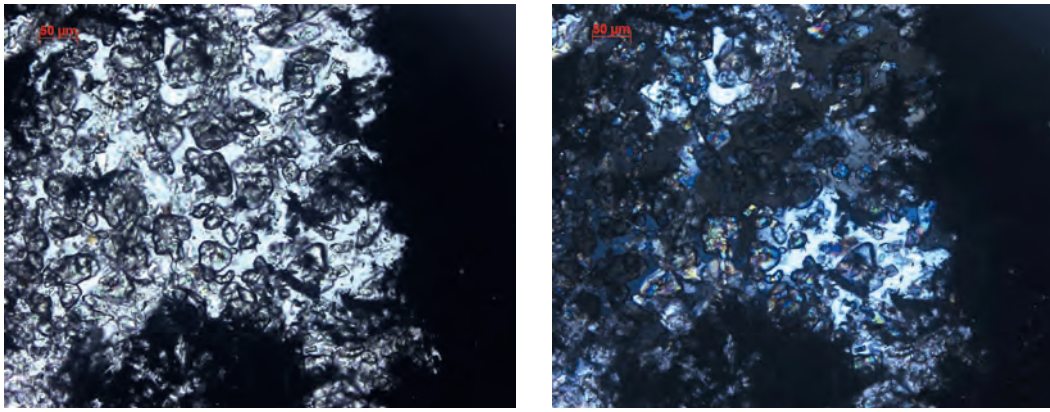

Fig. 12. Photomicrograph of pocket of monazite crystals in aggregate of acicular rutile. (a) Normal light, (b) crossed polars.

Monazite is a member of solid solution series (Ce,La,Nd...Sm)$[PO_4]$ (monazite proper) – $CaTh[PO_4]_2$ (brabantite) – $CaCe_2Th[PO_4]_4$ (cheralite) – $Th[SiO_4]$ (huttonite – gasparite (Ce,La,Nd)$[AsO_4]$ with a small admixture of the xenotime end-member $Y[PO_4]$ (Heinrich, 1962; Yushkin *et al.*, 1986; Pabst and Hutton, 1951; Bowie and Horne, 1953; Graeser and Schwander, 1977; Rose, 1980; Strunz and Nickel, 2001; Phosphates.., 2003). The usual Ce:La:Nd value in monazite is ~ 2:1:1, less frequent La is predominant, Nd is predominant occasionally. Monazite is typical of Ca-poor granite and syenite, granitic gneiss of normal and elevated alkalinity; it is the major carrier of *LREE*; content of Th is up to 30 wt.% and higher (Phosphates.., 2003; Philpotts and Ague, 2009). The content of U is also high in monazite of some granitic pegmatites (Gramaccioli and Segalstad, 1978). Th-free or Th-poor monazite occurs in hydrothermal rocks (Yushkin *et al.*, 1988; Phosphates.., 2003). When monazite is associated with xenotime, its composition is an indicator of temperature and pressure: at 2 kb, mole fraction of Y increases from 3 to 16% as temperature increases from 300 to 1000°C at 2 kb (Gratz and Heinrich, 1997).

Gumbeites monazite has not been studied before. In the Berezovsky gumbeite, it occurs as crystals of usual shape up to 45 µm in size, their clusters confined to deformed lamellae of ilmenite replaced by aggregates of acicular rutile (Figs. 11, 12). Monazite overgrows rutile and fill interstices between crystals of rutile (Fig. 13). It is intergrown with fluorapatite to form compromise growth surfaces. In phlogopite-magnesite gumbeite, this minerals is U-free and Th-poor (0.8–2.2 wt.% Th); Ce content is twice as much as that of La; the concentration of Nd is slightly less than that of La; content of Pr, Sm, and Dy is appreciable; small part of P is substituted by Si; content of the huttonite end-member is less than 2%. The compositions of five examined crystals of monazite are similar and correspond to the formula $(Ce_{0.40\text{-}0.43}La_{0.25\text{-}0.28}Nd_{0.16\text{-}0.18}Y_{0.02\text{-}0.05}Pr_{0.03\text{-}0.04}Sm_{0.02}Gd_{0.01\text{-}0.02}Eu_{0\text{-}0.01}Th_{0.01\text{-}0.02}Ca_{0.02})_{1\text{-}1.01}(P_{0.97\text{-}0.98}Si_{0.01\text{-}0.03})_{0.99\text{-}1}O_4$ (Table 11). These compositions are typical of monazite of high- to medium-temperature hydrothermal assemblages (Phosphates.., 2003).

The crystal cores of the Berezovsky monazite are enriched in Y (Table 11, anal. 81); the temperature of their and rims (anal. 84, 85) formation estimated from the Gratz-Heinrich equation (Gratz and Heinrich, 1997) is ca. 450°C and ca. 300°C, respectively.

Xenotime is a member of solid solution series $Y[PO_4]$ (xenotime proper) – *HREE*$[PO_4]$ including xenotime-(Yb) $Yb[PO_4]$. The content of the xenotime-(Y) end-member is 70–80% as usual; that of the *HREE*$[PO_4]$ is 15–25%, occasionally higher than 50%; the solid solution of high-temperature xenotime contains up to 5–10% of the (Ce,La,Nd...Sm)$[PO_4]$ end-member (monazite), up to 5% of the $CaTh[PO_4]_2$ (brabantite) – $CaCe_2Th[PO_4]_4$ (cheralite) end-member, and up to 5% of the (Th,U)$[SiO_4]$ end-member (thorite-coffinite) (Heinrich, 1962; Yushkin *et al.*, 1986; Gratz, and Heinrich, 1997; Strunz and Nickel, 2001; Phosphates.., 2003; Förster, 2006). Xenotime is a typical accessory mineral of various granitoids of normal and high alkalinity; it is the major carrier of *HREE* in them. It is rather abundant in high- and medium-temperature hydrothermal assemblages (Yushkin *et al.*, 1986; Phosphates.., 2003).

Gumbeitic xenotime has not been studied before. In the Berezovsky gumbeites, it occurs as small bipyramidal crystals and anhedral grains

Table 11. **Chemical composition (wt.%) of monazite from apopicritic phlogopite-magnesite gumbeites, Berezovsky deposit**

Component	81	82	83	84	85
Y_2O_3	2.40	1.41	1.33	1.18	1.04
La_2O_3	16.87	15.92	15.58	15.96	17.41
Ce_2O_3	29.58	30.73	30.36	29.43	30.60
Pr_2O_3	2.68	2.88	2.49	3.21	2.25
Nd_2O_3	11.64	12.59	13.39	12.38	12.09
Sm_2O_3	1.46	1.29	1.81	1.82	1.79
Eu_2O_3	0.36	0.23	0.27	0.10	0.16
Gd_2O_3	0.79	0.96	0.90	0.82	1.21
Tb_2O_3	bdl	0.16	0.06	0.16	0.11
Dy_2O_3	0.21	0.36	bdl	0.30	0.49
Ho_2O_3	bdl	bdl	bdl	0.16	bdl
Er_2O_3	0.18	0.15	bdl	bdl	0.15
Yb_2O_3	bdl	0.15	bdl	bdl	0.09
Lu_2O_3	bdl	0.09	0.17	bdl	0.19
ThO_2	2.20	1.41	1.41	2.23	0.83
TiO_2	0.21	0.26	0.21	0.18	0.24
UO_2	0.17	0.01	0.01	0.09	0.02
CaO	0.49	0.46	0.60	0.73	0.31
SrO	0.06	bdl	bdl	bdl	bdl
FeO	0.07	bdl	0.04	0.08	0.05
P_2O_5	30.35	30.63	30.91	30.72	30.70
SiO_2	0.66	0.37	0.50	0.48	0.34
Total	100.39	100.06	100.04	100.03	100.07
Atoms per formula unit (Total = 2)					
Y	0.05	0.03	0.03	0.02	0.02
La	0.27	0.26	0.25	0.26	0.28
Ce	0.40	0.42	0.43	0.41	0.42
Pr	0.04	0.04	0.03	0.04	0.03
Nd	0.16	0.17	0.18	0.17	0.16
Sm	0.02	0.02	0.02	0.02	0.02
Eu	0.01	–	–	–	–
Gd	0.01	0.01	0.01	0.01	0.02
Dy	–	–	–	–	0.01
Th	0.02	0.01	0.01	0.01	0.02
Ca	0.02	0.02	0.02	0.03	0.01
P	0.97	0.98	0.98	0.98	0.98
Si	0.03	0.01	0.02	0.02	0.01

Notes. A Camebax-microbeam electron microprobe, I.M. Kulikova analyst. Contents of Na and Tm are below detection limits.

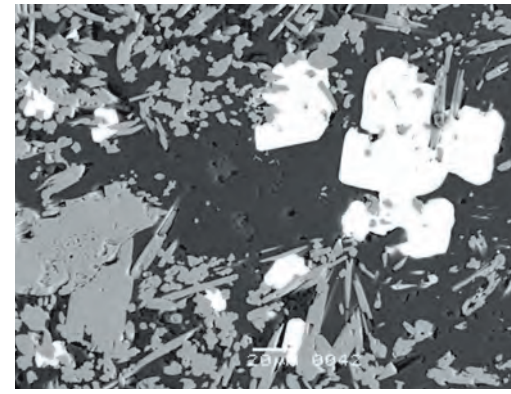

Fig. 13. Back-scattered electron image of crystal of monazite (white) in aggregate of rutile (gray), quartz, and micas (dark gray).

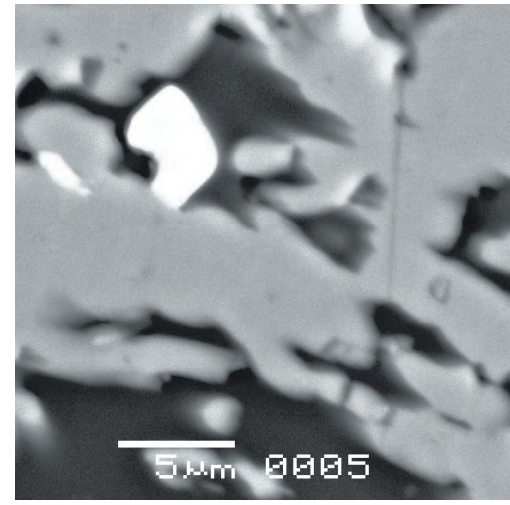

Fig. 14. Back-scattered electron image of crystal of xenotime (light) in aggregate of crystals of rutile (gray).

Fig. 15. Back-scattered electron image of anhedral xenotime (light) in aggregate of crystal of rutile (gray).

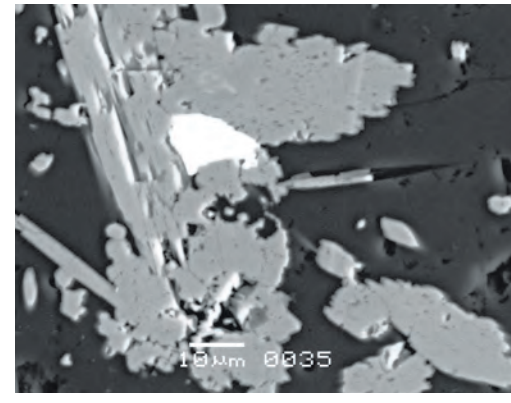

Table 12. **Chemical composition (wt.%) of xenotime from apopicritic phlogopite-magnesite gumbeites, Berezovsky deposit**

Component	86	87	88	89
Y_2O_3	42.87	41.42	39.78	39.24
La_2O_3	0.06	0.06	bdl	0.06
Ce_2O_3	0.45	0.44	0.29	0.30
Nd_2O_3	2.42	2.40	2.67	2.71
Sm_2O_3	2.07	2.05	2.51	2.55
Eu_2O_3	0.87	0.86	0.87	0.88
Gd_2O_3	3.56	3.52	5.45	3.54
Tb_2O_3	0.62	0.61	0.66	0.66
Dy_2O_3	4.45	4.43	5.09	5.17
Ho_2O_3	1.07	1.06	0.51	0.52
Er_2O_3	3.05	3.02	3.06	3.10
Tm_2O_3	0.24	0.24	0.27	0.27
Yb_2O_3	2.58	2.55	2.31	2.34
Lu_2O_3	0.40	0.40	0.54	0.55
TiO_2	0.18	0.25	0.14	0.14
UO_2	0.07	0.08	0.74	0.80
CaO	0.24	0.24	0.14	0.13
P_2O_5	35.53	35.33	34.94	34.07
SiO_2	0.24	0.22	0.31	0.22
Total	100.97	99.19	99.98	99.50
Atoms per formula unit (Total = 2)				
Y	0.75	0.74	0.71	0.71
Ce	0.01	0.01	-	-
Nd	0.03	0.03	0.03	0.03
Sm	0.02	0.02	0.03	0.03
Eu	0.01	0.01	0.01	0.01
Gd	0.04	0.04	0.06	0.06
Tb	0.01	0.01	0.01	0.01
Dy	0.05	0.05	0.06	0.06
Ho	0.01	0.01	0.01	0.01
Er	0.03	0.03	0.03	0.03
Yb	0.03	0.03	0.02	0.02
Lu	–	–	0.01	0.01
U	–	–	0.01	0.01
Ca	0.01	0.01	0.01	–
P	0.99	1.00	0.99	0.99
Si	0.01	0.01	0.01	0.01

Notes. A Camebax-microbeam electron microprobe, I.M. Kulikova analyst. Contents of Fe, Na, Sr, Pr, and Th are below detection limits.

up to 20 μm enclosed in clusters of acicular rutile (Figs. 14, 15). Xenotime in phlogopite-magnesite gumbeites is Th-free and U-poor (0.1−0.8 wt.% U); Y significantly predominates over *HREE*, the major of which are even with Dy≥Gd> Er>Yb. Nd and Sm are predominant of *LREE*; the content of Eu is greater than sum of Ce and La; only insignificant part of P is replaced with Si (Table 12). The composition of xenotime corresponds to the formula $(Y_{0.71-0.75}Dy_{0.05-0.06}Gd_{0.04-0.06}Er_{0.03}Nd_{0.03}Yb_{0.02-0.03}Sm_{0.02-0.03}Eu_{0.01}Tb_{0.01}Ho_{0.01}Lu_{0-0.01}Ca_{0-0.01})_{0.99-1}(P_{0.99-1}Si_{0.01})O_4$. Thus, xenotime from gumbeites contains 71−75% of the xenotime proper end-member, 17−20% of the *HREE*$[PO_4]$ end-member, 6−7% of the monazite end-member, and 1% of the coffinite end-member.

Thus, in the assemblage fluorapatite-monazite-zircon, U is concentrated in zircon; Th is concentrated in monazite and to some extent in zircon; *LREE* and most Y are incorporated into monazite that is significantly predominant over xenotime; the latter concentrates *HREE* and part of Y; fluorapatite is nearly *REE*-and actinide-free.

Talc is characteristic of the outer zone of metasomatic column. This mineral is Fe-poor with appreciable Ni; its composition is as follows (anal. 90; wt.%): SiO_2 62.51; MgO 30.88; FeO 0.81; MnO 0.02; NiO 0.38, total is 94.91 (N.N. Korotaeva analyst). Formula is $(Mg_{2.94}Fe_{0.04}Ni_{0.02})_3[(OH)_2/Si_4O_{10}]$.

Gersdorffite is a typical accessory mineral of phlogopite-magnesite gumbeites. In the green zone, the composition of gersdorffite corresponds to the formula $Ni_{0.98}Fe_{0.02}AsS$; in the yellow zone gersdorffite is Co-bearing $Ni_{0.87-0.93}Co_{0.07-0.12}Fe_{0.01}AsS$.

Comparison of apopicritic and other gumbeites

The described hight-temperature gumbeites replacing picrites contains assemblage magnesite-phlogopite-quartz, whereas high-temperature apogranitic gumbeites is present calcite-biotite-quartz. Gumbeites replacing picrite contains tourmaline that is absent in granitic gumbeite.

Comparison of apopicritic gumbeites and other types of metasomatites

Unlike listvenite, apopicritic gumbeites contains assemblages magnesite-phlogopite-quartz and magnesite-potassium feldspar-quartz, and monazite-(Ce), xenotime, zircon, fluorapatite, tourmaline, F-rich and Ba-bearing muscovite.

Talc-magnesite gumbeites contains phlogopite in contrast to talc-magnesite listvenites.

Unlike porphyry copper alterations, apopicritic gumbeites contains cogenetic monazite, zircon, and xenotime and does not contain magnetite (Lowell, Guilbert, 1970; Sillitoe, 2009). In adition the described alteration is accompanied with potassium feldspar-carbonate-quartz veins with scheelite or hematite (without magnetite and molybdinite) that is not typical of the porphyry copper alterations.

This study has been supported by the Russian Foundation for Basis Researches (project no. 13-05-00839).

References

Avdonin V.N. Apatite from sulfide-quartz veins of the Berezovsky deposit // Trudy GGI of the Ural Branch, AN SSSR. **1955**. Issue 26. P. 107–109 (in Russian).

Bellavin O.V., Vanshal O.V., Nirenshtein V.A. Shartash granite pluton, Middle Urals and related gold mineralization // Izv. AN SSSR. Ser. Geol. **1970**. N. 6. P. 86–90 (in Russian).

Borodaevsky N.I., Borodaevskaya M.B. Berezovsky gold field. Metallurgizdat. Moscow: **1947**. 247 p. (in Russian).

Borodaevsky N.I., Ershova N.A., Egorova N.A., Kazimirovsky N.F., Levitan G.M., Mikhailova L.V., Samartsev I.T. Berezovsky deposit // Gold deposits of the USSR. V. 1. Moscow. TSNIGRI. **1984**. P. 7–53 (in Russian).

Bowie S.H.U., Horne J.E.T. Cheralite, a new mineral of the monazite group // Mineral. Mag. **1953**. Vol. 30. P. 93–99.

Bushlyakov I.N., Sobolev I.D. Petrology, mineralogy, and geochemistry of Upper Iset' granitoid pluton at Urals. Moscow: Nauka. **1976**. 340 p. (in Russian).

Chesnokov B.V., Kotybaeva N.N., Bushmakin A.F. Endogenic minerals of bismuth and nickel at Berezovsky gold deposit in Middle Urals // Tr. Mining and Geology Institute, Ural Branch AN SSSR. **1975**. Issue 106. P. 123–126 (in Russian).

Ershova N.A., Levitan G.M. Relation of gold mineralization to granitic rocks: case of Shartash pluton, Middle Urals // Tr. TsNIGRI. **1978**. Issue 136. P. 76–92 (in Russian).

Fershtater G.B. Structural and formation zoning of Urals and magmatism. Geotectonika. **1992**. N. 6. P. 3–17 (in Russian).

Fershtater G.B., Borodina N.S., Rapoport M.S., Osipova T.A., Smirnov V.N., Levin V.Ya. Orogenic granitoid magmatism of Urals // Ural Branch, Russian Academy of Sciences. Miass. **1994**. 250 p. (in Russian).

Förster H.-J. Composition and origin of intermediate solid solution in the system thorite – xenotime – zircon – coffinite // Lithos. **2006**. Vol. 88. P. 35–55.

Frondel C., Collette R.L. Hydrothermal synthesis of zircon, thorite and hattonite // Amer. Mineral. **1957**. Vol. 42. P. 759–765.

Graeser S., Schwander H. Gasparite-(Ce) and monazite-(Nd): Two new minerals to the monazite group from the Alps // Schweiz. Mineral. Petrogr. Mitt. **1977.** Bd. 67. S. 103–113.

Gramaccioli C.M., Segalstad T.V. A uranium- and thorium-rich monazite from a south-alpine pegmatite at Piona, Italy // Amer. Mineral. **1978.** Vol. 63. P. 757–761.

Gratz R., Heinrich W. Monazite – xenotime thermobarometry: Experimental calibration of the miscibility gap in the binary system $CePO_4$ – YPO_4 // Amer. Mineral. **1997**. Vol. 82. P. 772–780.

Heinrich E.W. Mineralogy and geology of radioactive raw materials. McGraw-Hill Book Co. Inc., New York. **1958**.

Ivanov A.A. Geology of primary gold deposits in the Urals // 200 years of gold industry. Sverdlovsk. Metallurgizdat. **1948**. P. 127–168 (in Russian).

Karpinsky A.P. Major typical rocks hosting lode gold deposits in Berezovsky mining district // Izv Geol. Comm. **1887**. Vol. VI. N. 12. P. 475–478 (in Russian).

Kholodnov V.V., Bushlyakov I.N. Halogens in endogenic ore formation. Institute of Geology and Geochemistry, Ural Branch. Russian Academy of Sciences. Yekaterinburg. **2002.** 395 p. (in Russian).

Koptev-Dvornikov V.S. Problem of magmatic petrography regarded with formation of hydrothermal deposit // Magmatizm and related minerals. Moscow. AN SSSR. **1955**. P. 22–44 (in Russian).

Korzhinsky D.S. Studies of metasomatic processes // Principle problems in doctrine of magmatic-related ore deposits. Moscow. AN SSSR. **1953**. P. 334–456 (in Russian).

Krasnobaev A.A. Zircon as indicator of geological processes. Moscow. Nauka. **1986.** 152 p. (in Russian).

Kurulenko R.S., Trayanova M.V., Kobuzov A.S., Yablonskaya L.V. Scheelite from quartz veins of the Shartash pluton // Ann. Report-1983, Institute of Geology and Geochemistry, Ural

Scientific Center AN SSSR. Sverdlovsk. **1984**. P. 104–105 (in Russian).

Kutyukhin P.I. Conditions of localization of ores in veins of Berezovsky deposit // 200 years of gold industry. Metallurgizdat, Sverdlovsk, **1948**. P. 249–275 (in Russian).

Kutyukhin P.I. Mineralogy of ores at Berezovsky gold deposit and types of quartz veins. Sverdlovsk Mining Institute. Sverdlovsk. **1937.** 93 p. (in Russian).

Laipanov Kh.Kh., Mikhailova L.V. Mineralogical and geochemical features of listvenites, beresites, and gold-bearing quartz veins // Tr. TsNIGRI, **1982**. N. 167. P. 49–54 (in Russian).

Levitan G.M., Ershova N.A., Rapoport M.S., Vigorova V.G., Grabezhev A.I., Chashchukhina V.A. Granitoid assemblages of Eastern slope of Middle and Southern Urals // Soviet Geology. **1979**. N. 12. P. 42–56 (in Russian).

Lowell J.D., Guilbert J.M. Lateral and vertical alteration-mineralization zoning in porphyry ore deposits // Econ. Geol. **1970**. Vol. 65. P. 373–408.

Matveev K.K. Gumbeika tungsten deposit // Doklady AN SSSR. Ser. A. **1928**. N. 8. P. 128–132 (in Russian).

Ovchinnikov L.N., Voronovsky S.N., Malyarova G.V. New data on absolute age of Phanerosoic ore deposits // Determination of absolute age of ore deposits and young magmatic rocks. Moscow. Nedra. **1976**. P. 17–26 (in Russian).

Pabst A., Hutton C.O. Huttonite, a new monoclinic thorium silicate with an account on its occurrence, analysis, and properties // Amer. Mineral. **1951.** Vol. 36. P. 60–69.

Peng G., Lurh J.F., McGee J.J. Factor controlling sulfur concentrations in volcanic apatite // Amer. Mineral. **1997.** Vol. 82. P. 1210–1224.

Philpotts A.R., Ague J.J. Principles of igneous and metamorphic petrology. Cambridge: Cambridge University Press. **2009**. 667 p.

Phosphates: Geochemical, geobiological and materials importance / Eds. *Kohn M.L., Rakovan J., Hughes J.M.* // Rev. Mineralogy Geochemistry. **2003.** Vol. 48. 742 p.

Pribavkin S.V., Montero P., Bea F, Fershtater G.B. U-Pb age of rocks and mineralization of Berezovsky gold deposit, Middle Urals // Report-2011, Institute of Geology and Geochemistry, Ural, Ural Branch, Russian Academy of Sciences, **2012**. P. 213–217 (in Russian).

Puchkov V.N. Geology of Urals and Ural region. Institute of Geology, Ufa Scientific Center, Russian Academy of Sciences. Ufa. **2010**. 280 p. (in Russian).

Rapoport M.S., Babenko V.V., Boltyrov V.B. Berezovsky gold deposit // Izv. VUZov. Mining J. **1994**. N. 6. P. 86–96 (in Russian).

Rose D. Brabantite, $CaTh(PO_4)_2$, a new mineral of the monazite group // Neues Jahrb. Mineral. Monat. **1980**. S. 247–257.

Rubin J.N., Henry C.D., Price J.G. Mobility of zirconium and other "immobile" elemets during hydrothermal alteration // Chem. Geol. **1993**. Bd. 110. S. 29–47.

Sazonov V.N. Beresite-listvenite assemblage and related mineralization: case of Urals. Ural Scientific Center AN SSSR, Sverdlovsk. **1984**. 208 p. (in Russian).

Shteinberg D.S. Kedrovka scheelite deposit // Sov. Geology. **1939**. N. 2. P. 85–89 (in Russian).

Shteinberg D.S., Ronkin Yu.L., Kurulenko R.S., Lepekhina O.P., Berseneva N.P. Rb/Sr age of Shartash intrusive complex // Ann. Report-1988, Institute of Geology and Geochemistry, Ural Branch. Sverdlovsk. AN SSSR. **1989**. P. 110–112 (in Russian).

Sillitoe R.H. Porphyry copper systems // Econ. Geol. **2009**. Vol. 104. P. 3–41.

Sobolev I.D. Brief review of geological structure of district of Upper Iset', Shartash, Adui, and Shilovo-Konevsky granitoid plutons. Institute of Geology and Geochemistry, Ural Scientific Center AN SSSR, Sverdlovsk. **1966.** 97 p. (in Russian).

Spiridonov E.M. Caledonian inversion plutonogenic gold-quartz assemblage of Central Kazakhstan // Geol. Ore. Deposits. **1995**. Vol. 37. N. 3. P. 179–207 (in Russian).

Spiridonov E.M. Listvenites and zodites // Internal. Geol. Rev. **1991**. Vol. 33. № 4. P. 397–407.

Spiridonov E.M., Baksheev I.A., Seredkin M.V., Prokof'ev V.Yu., Ustinov V.I., Filimonov S.V. Gumbeites and Associated Ore Mineralization of the Urals (Russia) // Geol. Ore Deposits. **1998$_1$**. Vol. 39. N. 2. P. 152–171 (in Russian).

Spiridonov E.M., Barsukova N.S., Baksheev I.A., Pletnev P.A., Seredkin M.V. Transformation of primary chrome spinels from ultramafic rocks of Nurali, Bazhenovo, and Karabash massifs, and small bodies of Berezovsky and Gumbeika deposits in Urals // Ural Summer Mineralogical School-97, Ural State Mining and Geology Academy, Yekaterinburg. **1997$_1$**. P. 23–27 (in Russian).

Spiridonov E.M., Barsukova N.S., Pletnev P.A. Zn-rich chrome spinels // Mineralogy of

Urals. Vol. II, Miass. **1998$_2$**. P. 127–129 (in Russian).

Spiridonov E.M., Naz'mova G.N., Sokolova N.F., Shalaev Yu.S. Composition and evolution of granodiorite and early orogenic monzonite complexes of Urals and Kazakhstan and related metasomatic rocks and ores (Mg skarn, Ca skarn, K propylite, quartz-sericite, Na propyllite, gumbeite, beresite and listvenite, and argillic alteration) // Magmatizm, metamorphism, and deep-seated structure of Urals. Part 2. Institute of Geology and Geochemistry, Ural Branch, Russian Academy of Sciences. Yekaterinburg. **1997$_2$**. P. 208–211 (in Russian).

Spiridonov E.M., Nurmukhametov F.M., Korotaeva N.N., Kulikova I.M., Sidorova N.V. Late magmatic allanite-(Ce) in gold-bearing granitoids of Shartash pluton, Middle Urals // Ural Geol. J. **2013**. N. 3. P. 46–55 (in Russian).

Spiridonov E.M., Pletnev P.A. Metasomatic rocks of beresite-listvenite assemblage of Zolotaya Gora, Karabsh Mount // Ural Geol. J. **2002**. N. 3. P. 37–47 (in Russian).

Spiridonov E.M., Zhernakov V.I., Baksheev I.A., Savina D.N. Typomorphism of talc from apoultramafic metasomatites of the Urals // Dokl. RAS. **2000**. Vol. 372. N. 4. P. 737–739.

Strunz H., Nickel E.H. Strunz mineralogical tables. Chemical structural mineral classification system. Stutgart: E. Schweizerbart'sche Verlagsbuchhandlung. **2001.** 870 S.

Votyakov S.L., Shchapova Yu.V., Khiller V.V. Crystal chemistry and physics of radiation-thermal effects in some U- and Th-bearing minerals as base for chemical dating. Ural Branch Russian Academy of Sciences. Yekaterinburg. **2011.** 336 p. (in Russian).

Yushkin N.P., Ivanov O.K., Popov V.A. Introduction to topomineralogy of Urals. Moscow: Nauka. **1986**. 294 p. (in Russian).

Zircon / Eds. *Hanclar J.M., Hoskin P.W.O.* // Rev. Mineral. Geochem. **2004.** Vol. 53. 500 p.